Polarimetric Radar Rain Estimation through Retrieval of Drop Size Distribution Using a Bayesian Approach

QING CAO

Atmospheric Radar Research Center, University of Oklahoma, Norman, Oklahoma

GUIFU ZHANG

School of Meteorology, and Atmospheric Radar Research Center, University of Oklahoma, Norman, Oklahoma

EDWARD A. BRANDES

National Center for Atmospheric Research, Boulder, Colorado*

TERRY J. SCHUUR

Cooperative Institute for Mesoscale Meteorological Studies, University of Oklahoma, and NOAA/OAR/NSSL, Norman, Oklahoma

(Manuscript received 19 March 2009, in final form 18 December 2009)

ABSTRACT

This study proposes a Bayesian approach to retrieve raindrop size distributions (DSDs) and to estimate rainfall rates from radar reflectivity in horizontal polarization Z_H and differential reflectivity Z_{DR}. With this approach, the authors apply a constrained-gamma model with an updated constraining relation to retrieve DSD parameters. Long-term DSD measurements made in central Oklahoma by the two-dimensional video disdrometer (2DVD) are first used to construct a prior probability density function (PDF) of DSD parameters, which are estimated using truncated gamma fits to the second, fourth, and sixth moments of the distributions. The forward models of Z_H and Z_{DR} are then developed based on a T-matrix calculation of raindrop backscattering amplitude with the assumption of drop shape. The conditional PDF of Z_H and Z_{DR} is assumed to be a bivariate normal function with appropriate standard deviations. The Bayesian algorithm has a good performance according to the evaluation with simulated Z_H and Z_{DR}. The algorithm is also tested on S-band radar data for a mesoscale convective system that passed over central Oklahoma on 13 May 2005. Retrievals of rainfall rates and 1-h rain accumulations are compared with in situ measurements from one 2DVD and six Oklahoma Mesonet rain gauges, located at distances of 28–54 km from Norman, Oklahoma. Results show that the rain estimates from the retrieval agree well with the in situ measurements, demonstrating the validity of the Bayesian retrieval algorithm.

1. Introduction

For decades, weather radars have played a significant role in quantitative precipitation estimation (QPE). The conventional approach to QPE has mostly been to implement a power-law relation between radar reflectivity Z and rainfall rate R. Over the years, many Z–R relations that vary according to rain type, intensity, season, and region (summarized by Rosenfeld and Ulbrich 2003) have been developed and used. For example, the current National Weather Service Weather Surveillance Radar-1988 Doppler (WSR-88D) applies two different Z–R relations: $Z = 300R^{1.4}$ for midlatitude rain and $Z = 250R^{1.2}$ for tropical rain. It is well recognized that raindrop size distribution (DSD) variability is a major source of the diversity of Z–R relations (e.g., Sachidananda and Zrnić 1987; Brandes et al. 1999; Steiner et al. 2004; Lee and Zawadzki 2005). Recent studies have shown that the

* The National Center for Atmospheric Research is sponsored by the National Science Foundation.

Corresponding author address: Qing Cao, Atmospheric Radar Research Center, University of Oklahoma, 1200 David L. Boren Blvd., Suite 4638, Norman, OK 73072.
E-mail: qingcao@ou.edu

DOI: 10.1175/2009JAMC2227.1

use of polarimetric radar data (PRD) has the potential to significantly improve rainfall estimation (e.g., Zhang et al. 2001; Brandes et al. 2002; Ryzhkov et al. 2005b; Lee 2006; Cao et al. 2008). In addition to radar reflectivity in horizontal polarization Z_H, polarimetric measurements, such as differential reflectivity Z_{DR} and specific differential phase K_{DP}, provide valuable information that can be used to resolve problems caused by DSD variability, hail contamination, beam blockage, and other sources of error. As a consequence, the application of PRD helps reduce the uncertainty in rain estimation.

Polarimetric rainfall estimators are primarily developed through PRD simulations that are based on either simulated or measured DSDs. Rainfall relations depend on different assumptions, datasets, and fitting procedures. For example, one of the essential assumptions is the raindrop shape. Many shape models—such as the equilibrium shape model by Beard and Chuang (1987), the oscillating shape model by Bringi et al. (2003), and the experimental shape model by Brandes et al. (2002)—have been proposed. Different raindrop shape models might lead to different values of PRD for any given DSD. Brandes et al. (2002) illustrated this with an example in which the Z_{DR} simulated using the equilibrium shape model was 0.2 dB larger than the Z_{DR} calculated using the experimental shape model. It is worth noting that no consensus currently exists within the community regarding which raindrop shape model should be used. Any shape model used might contain errors that result in radar variable estimates that are less than optimal. Consequently, to mitigate the model error attributed to various factors, discrepancies between calculated PRD and real PRD need to be reduced by an appropriate adjustment.

If we assume ground measurements to be a good approximation of the in situ conditions aloft, then disdrometer measurements can be used to calibrate PRD (e.g., Brandes et al. 2002; Lee and Zawadzki 2006). The primary advantage of this method is that it maintains a consistency between the real PRD and the calculated PRD. Therefore, the rainfall estimator developed from the PRD simulated using disdrometer measurements could be applicable to real PRD. A limitation of this method is that a large difference between radar and disdrometer sampling volumes might cause measurement mismatches that could result in a calibration bias (e.g., Cao et al. 2008). Precipitation inhomogeneity within a radar resolution volume, however, is typically not substantial for ranges less than 30 km and/or in quasi-uniform (e.g., stratiform) precipitation, which has a slow temporal variability. Temporal averaging can further reduce the rainfall variability that might be large at small time scales (Ciach and Krajewski 2006). For these reasons, the error effect due to different sampling volumes is small, and the disdrometer can be accepted as an effective calibration tool. Another concern is the quality of PRD. Contamination from snow or hail, clutter, anomalous propagation, and biological objects would lead to inaccurate rainfall estimation. Contaminated PRD should, therefore, be rejected and not used for the calibration.

The performance of rain estimators is also affected by radar measurement error (e.g., Ryzhkov et al. 2005a). Many empirical relations employing PRD—for example, $R(Z_H, Z_{DR})$, $R(K_{DP})$, and $R(Z_H, Z_{DR}, K_{DP})$—have been reported previously in the literature (e.g., Brandes et al. 2003; Ryzhkov et al. 2005b; Lee 2006). These deterministic estimators calculate the rainfall rate directly from PRD without accounting for any error effect. Because measurement error is an inevitable obstacle to the accuracy of rain estimator, quantifying the error effect and optimizing the use of radar measurements becomes an important issue. Bayesian theory offers a promising method of achieving this goal (e.g., Evans et al. 1995; McFarlane et al. 2002; Di Michele et al. 2005; Chiu and Petty 2006). Hogan (2007) presented an example of how a Bayesian approach can be applied spatially. Although the variational method is believed to be a promising method of using PRD, the implementation is complicated and many issues remain to be resolved. For example, Hogan (2007) applied Z_H as a strong constraint; that is, Z_H was not optimally used and its error was ignored in the variational scheme. He applied several empirical relations for the construction of forward models, which heavily depend on Z_H. The errors attributed with the empirical relations and the error propagation of Z_H might degrade the process of optimization. On the other hand, high-order DSD models (e.g., gamma DSD) have been shown to represent rain physics well. Application of a variational scheme to those models, however, is complicated. For this reason, Hogan (2007) simplified his two-parameter rainfall-rate retrieval scheme to improve efficiency. First, for each consecutive 10 gates, he only assumed a simple Z_H–R power-law relation. Second, only one state parameter—the coefficient of the power-law relation—was optimally retrieved. Whereas Hogan (2007) applied a Bayesian approach spatially, in the current study we apply the Bayesian approach temporally, using historic data as the prior information to optimally retrieve two parameters of a constrained-gamma (C-G) DSD model simultaneously from two PRD. Considering the significance of DSDs in rain microphysics, DSD parameters, rather than integral parameters such as rainfall rate, are treated as state parameters. The algorithm uses Z_H and Z_{DR}, the two polarimetric radar variables with the highest data quality. With prior information derived from historic DSD data, the algorithm searches the state

parameter estimates with the maximum probability and, consequently, the rain parameter with the maximum probability. The result provides not only mean values of the state parameters but also their standard deviations, which determine the reliability of estimation. For example, when Z_{DR} has a negative value, the Bayesian approach produces a rainfall rate with a large standard deviation, implying a large measurement error of data. It is worth noting that two factors are required for the success of the Bayesian approach. The first and most important factor is the quality of the prior information on rain characteristics. The second factor is the appropriate use of state parameters and conditional probabilities, as well as the forward models. In this study, we assume DSDs measured by the disdrometer provide a ground truth of rain property. Large datasets of disdrometer measurements are then used to construct the prior distribution of the state parameters. The state parameters and the forward models will be described in detail in section 3.

Various DSD models have been applied in previous studies (e.g., Marshall–Palmer, exponential, lognormal, gamma, and normalized gamma forms). The gamma distribution, with a flexible functional shape, is usually thought to represent natural DSD variability well. The distribution is written as

$$N(D) = N_0 D^{\mu} \exp(-\Lambda D), \tag{1}$$

where $N(D)$ denotes the DSD, N_0 ($\text{mm}^{-1-\mu}\ \text{m}^{-3}$) denotes the number concentration parameter, μ denotes the distribution shape parameter, Λ (mm^{-1}) denotes the slope parameter, and D (mm) denotes the equivalent volume diameter. To facilitate DSD retrieval from radar-measured Z_H and Z_{DR}, Zhang et al. (2001) proposed a C-G model with a constraining μ–Λ relation derived from disdrometer measurements. There have been many successful applications of the C-G model (e.g., Brandes et al. 2004a,b; Vivekanandan et al. 2004; Zhang et al. 2006; Cao et al. 2008). In this study, an updated constraining relation by Cao et al. (2008) is used for DSD retrieval, and its functional form is

$$\mu = -0.0201\Lambda^2 + 0.902\Lambda - 1.718. \tag{2}$$

It is not clear how radar variables other than Z_H and Z_{DR} can be used to improve DSD retrieval. For example, although K_{DP} has been used to retrieve DSD parameters (e.g., Gorgucci et al. 2002), Brandes et al. (2004a) showed that the deterioration caused by K_{DP} error might outweigh the contribution by K_{DP}. Moreover, K_{DP}, when smoothed over a long distance to reduce the noise effect, might not be consistent with Z_H and Z_{DR}, which are measured at every gate and not smoothed as much. Because of these considerations, only two radar variables (Z_H and Z_{DR}) and a two-parameter model (C-G model) have been used for the Bayesian retrieval.

In this study, we present rain estimation using a Bayesian approach to retrieve DSD parameters from Z_H and Z_{DR} at S band (10.7 cm). In addition to the evaluation by simulated radar data, a rain event on 13 May 2005 in central Oklahoma is analyzed to verify the algorithm by comparing radar retrievals with in situ measurements. The study is organized as follows: Section 2 describes the dataset measured by three disdrometers, one polarimetric radar, and six rain gauges. The Bayesian approach methodology is introduced in section 3 and evaluated using the disdrometer dataset in section 4. A case study is presented in section 5, and conclusions are provided in the last section.

2. Data description

Because of their ability to directly measure raindrop spectra, disdrometers are of fundamental importance to the study of rain microphysics (e.g., Schuur et al. 2001; Zhang et al. 2001, 2008). In this study, we use data collected by a two-dimensional video disdrometer (2DVD; Kruger and Krajewski 2002), which can measure the size and fall speed of individual raindrops and, under most environmental conditions, accurately reproduce rain DSDs. The design of the 2DVD, which has a sampling area of approximately 10 cm $\times$ 10 cm, has evolved over the years with the resolution of the prototype model having a resolution of 0.195 mm and the more recent models having a resolution of 0.132 mm. From 2005 to 2007, more than 30 000 min of 2DVD data were collected at four locations—named ''Harris,'' Kessler Farm Field Laboratory (''KFFL''), ''Jessup,'' and Norman (''KOUN'') in Fig. 1—in central Oklahoma. These data came from three 2DVDs, which were operated by the University of Oklahoma, National Center for Atmospheric Research (NCAR), and National Severe Storms Laboratory (NSSL). We assume that the >30 000 DSDs measured by these 2DVDs provide sufficient statistical information on rain physics in Oklahoma.

A squall line that passed through central Oklahoma from the northwest to the southeast on 13 May 2005 is examined in this study to illustrate the Bayesian retrieval algorithm. The radar data were collected by the KOUN radar, which is an S-band polarimetric WSR-88D with a beamwidth of 0.95° and a range resolution of 250 m. To verify the rain retrieval from radar measurements, rain gauge measurements from six Oklahoma Mesonet sites have been used. The six sites—Spencer (SPEN), Minco (MINC), Chickasha (CHIC), Ninnekah (NINN),

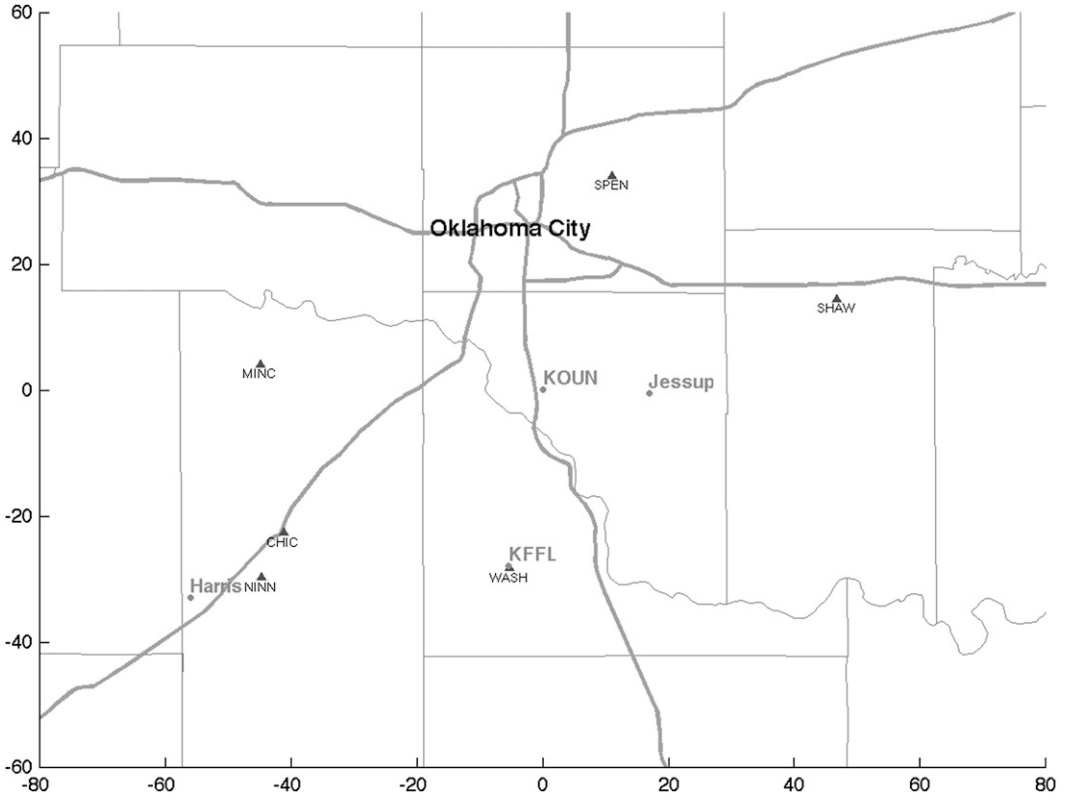

FIG. 1. Location of instrumentation used in this study. KOUN radar is indicated by a dark point. Six Oklahoma Mesonet sites are indicated by dark triangles. Three disdrometer sites are indicated by gray points, and the other disdrometer site is located at KOUN.

Washington (WASH) and Shawnee (SHAW)—are located 35.7 km north, 45.0 km west, 47.0 km southwest, 53.6 km southwest, 28.7 km south, and 48.8 km east of KOUN, respectively (denoted by triangles in Fig. 1). The standard rain gauge used by the mesonet has a sampling area of approximately 0.07 m^2. According to Ciach (2003) and Habib et al. (2001), the rainfall measurement error of a rain gauge depends on rainfall intensity and time scale. With accumulated rainfall being recorded every 5 min, the accuracy of the rain gauge is approximately $\pm 5\%$ over the range of 0–50 mm h^{-1}. On 13 May 2005, the NCAR 2DVD was located at KFFL, which is approximately 300 m from WASH. A comparison of 2DVD and rain gauge measurements in section 5 will show the consistency between these two instruments.

Figure 2 shows the plan position indicator (PPI) image of KOUN radar data at 0830 UTC 13 May 2005. The leading convective line was followed by a large region of stratiform precipitation. Convective cores had Z_H as large as 55 dBZ and Z_{DR} as large as 3.5 dB. The PPI scans were made at an elevation of 0.5°. The radar beam center was 250 m above the NCAR 2DVD at the range of 28.4 km. Figure 2 also shows the cross-correlation coefficient ρ_{HV} and the result of a fuzzy-logic hydrometeor classification algorithm developed by NSSL (Schuur et al. 2003; Ryzhkov et al. 2005c).

3. Methodology

a. Bayesian approach

In the Bayesian approach as implemented here, $\mathbf{x}$ is a state vector, representing the rain physics that need to be retrieved from the radar measurement; and $\mathbf{y}$ is the measurement vector. According to the Bayesian theorem, the posterior conditional probability density function (PDF) $P_{post}(\mathbf{x}|\mathbf{y})$ is given by

$$P_{\text{post}}(\mathbf{x}|\mathbf{y}) = \frac{P_f(\mathbf{y}|\mathbf{x})P_{\text{pr}}(\mathbf{x})}{\int P_f(\mathbf{y}|\mathbf{x})P_{\text{pr}}(\mathbf{x})\,d\mathbf{x}}, \tag{3}$$

where $P_{pr}(\mathbf{x})$ is the prior PDF of state $\mathbf{x}$, and $P_f(\mathbf{y}|\mathbf{x})$ is the conditional PDF of observation $\mathbf{y}$ given a state $\mathbf{x}$. Given an observation $\mathbf{y}$, the expected value and the standard deviation of state $\mathbf{x}$ are then calculated by integrating over the entire range of $\mathbf{x}$:

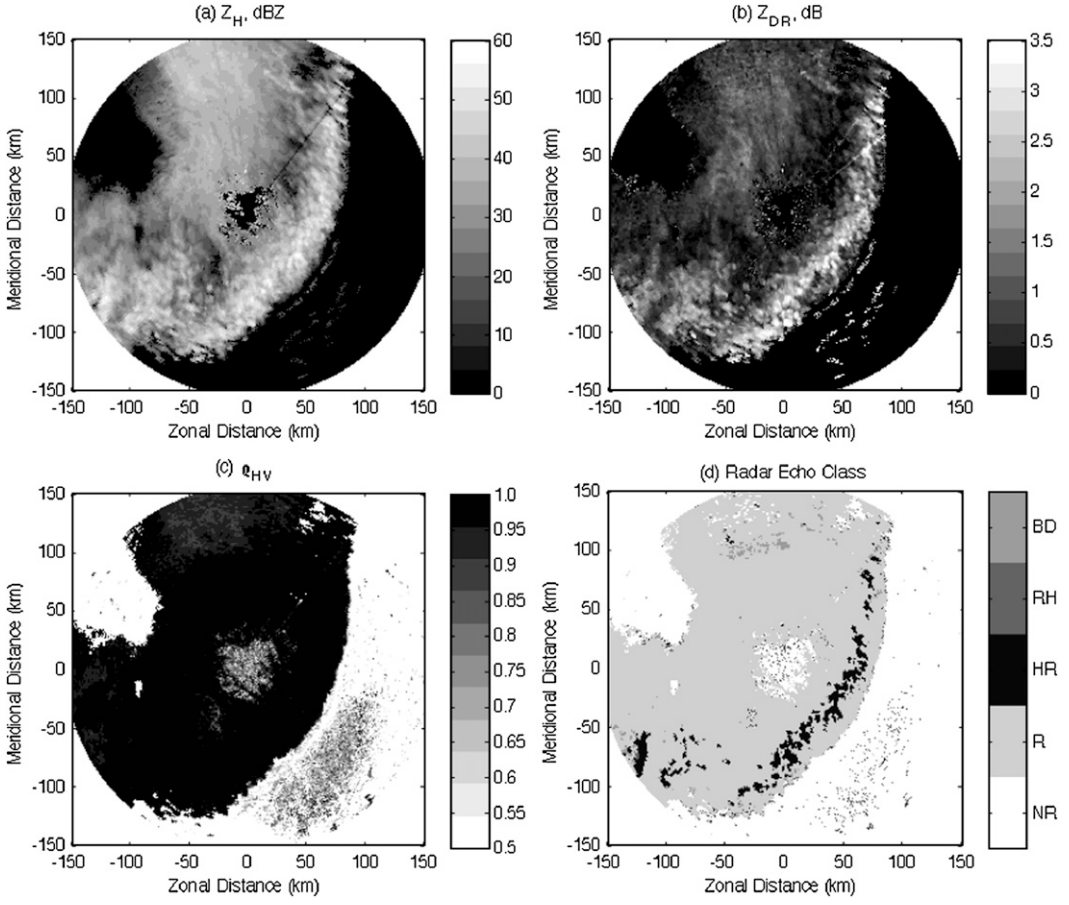

FIG. 2. PPI image of KOUN radar observations at 0830 UTC 13 May 2005: (a) Z_H (dBZ), (b) $Z_{\rm DR}$ (dB), (c) $\rho_{\rm HV}$, and (d) radar echo classification. Classes are defined as NR: nonrain echo, R: rain; HR: heavy rain, RH: rain and hail mixture, and BD: big drop.

$$E(\mathbf{x}|\mathbf{y}) = \frac{\int \mathbf{x} P_f(\mathbf{y}|\mathbf{x}) P_{\rm pr}(\mathbf{x})\, d\mathbf{x}}{\int P_f(\mathbf{y}|\mathbf{x}) P_{\rm pr}(\mathbf{x})\, d\mathbf{x}} \quad \text{and} \tag{4}$$

$$\mathrm{SD}(\mathbf{x}|\mathbf{y}) = \left\{ \frac{\int [\mathbf{x} - E(\mathbf{x})]^2 P_f(\mathbf{y}|\mathbf{x}) P_{\rm pr}(\mathbf{x})\, d\mathbf{x}}{\int P_f(\mathbf{y}|\mathbf{x}) P_{\rm pr}(\mathbf{x})\, d\mathbf{x}} \right\}^{1/2}, \tag{5}$$

where $E(\cdot)$ and $\mathrm{SD}(\cdot)$ denote a conditional expected value and standard deviation, respectively. For convenience, we have omitted the conditional terms and written them as $E(\mathbf{x})$ and $\mathrm{SD}(\mathbf{x})$ hereinafter. We set $\mathbf{x} = (N_0', \Lambda')$ and $\mathbf{y} = (Z_H, Z_{\rm DR})$, where $N_0' = \log_{10} N_0\, [\log_{10}(\mathrm{mm}^{-1-\mu}\, \mathrm{m}^{-3})]$ and $\Lambda' = \Lambda^{1/4}\, (\mathrm{mm}^{-1/4})$. A detailed analysis of state variable is presented in section 3c.

b. The forward model

The forward model is used to calculate polarimetric radar variables from DSD parameters. Several assumptions are made for the calculation. First, we assume the radar wavelength is 10.7 cm (S band), the raindrop temperature is 10°C, and the standard deviation of the raindrop's canting angle is 0. Then, we assume the raindrop shape follows the relation proposed by Brandes et al. (2002, 2005), that is, the experimental shape model. Under these assumptions, Z_H, radar reflectivity at vertical polarization Z_V, and $Z_{\rm DR}$ are calculated as

$$Z_{H,V} = \frac{4\lambda^4}{\pi^4 |K_w|^2} \int_0^\infty |f_{a,b}(\pi)|^2 N(D)\, dD,$$

$$Z_{H,V}(\mathrm{dB}) = 10 \log_{10} Z_{H,V}, \quad \text{and} \tag{6}$$

$$Z_{\rm DR}(\mathrm{dB}) = 10 \log_{10}(Z_H / Z_V), \tag{7}$$

where $f_a(\pi)$ and $f_b(\pi)$ represent the backscattering amplitude for horizontal and vertical polarization, respectively; λ is the wavelength; $K_w = (\varepsilon_r - 1)(\varepsilon_r + 2)^{-1}$; and ε_r is the complex dielectric constant of water. Here, $f_a(\pi)$ and $f_b(\pi)$ have been calculated based on the T-matrix

method (e.g., Zhang et al. 2001). Results of calculated scattering amplitudes have been stored as a lookup table with regard to a number of equivalent diameters. The lookup table provides a convenient way to calculate radar variables given a DSD. To evaluate the Bayesian DSD retrieval, integral rain variable R (mm h^{-1}) and mean volume diameter D_m (mm) are calculated as follows:

$$R = \frac{\pi}{6}\int_0^\infty D^3 N(D) v(D)\, dD \quad \text{and} \tag{8}$$

$$D_m = \frac{\int_0^\infty D^4 N(D)\, dD}{\int_0^\infty D^3 N(D)\, dD}, \tag{9}$$

where v is the empirical terminal velocity proposed by Brandes et al. (2002).

c. The prior distribution of DSD parameters

The key to the Bayesian approach is the construction of *a prior* PDF of state parameter $P_{\text{pr}}(\mathbf{x})$, which is used in Eqs. (4) and (5). To do so, we first assume the DSDs measured by a 2DVD follow the form of gamma function [Eq. (1)]. The gamma function parameters—N_0, Λ, and μ—are then obtained by fitting each measured DSD and used to construct *a prior* PDF. The fitting procedure follows the truncated moment fit described by Vivekanandan et al. (2004), which utilizes the second, fourth, and sixth DSD moments. Assuming the DSD follows a gamma distribution, DSD parameters estimated by the moment method would have a bias (e.g., Zhang et al. 2003; Smith et al. 2009); however, considering the model error (i.e., a nongamma DSD) and measurement error, Cao and Zhang (2009) have demonstrated that the method using the second, fourth, and sixth moments is an appropriate approach compared to other moment methods, the maximum likelihood, and L-moment methods.

Distributions of estimated N_0 and Λ are found to be greatly skewed and have a large dynamic range (not shown). It is obviously not appropriate to directly use N_0 and Λ as the state parameters. For example, the dynamic range of Λ is small for heavy or moderate rain, while it is large for light rain, which has a large Λ. Physical properties (e.g., rainfall rate, DSD moments) vary nonlinearly with increasing Λ. It is, therefore, necessary to transform the evaluation range to distinguish different physical processes. To reduce their dynamic ranges and mitigate nonlinear effects, $N_0' = \log_{10} N_0$ and $\Lambda' = \Lambda^{1/4}$ are used here. Occurrence histograms of N_0' and Λ' are shown in Fig. 3. The dynamic ranges of N_0' and Λ' for light rain are reduced significantly, compared to the ranges

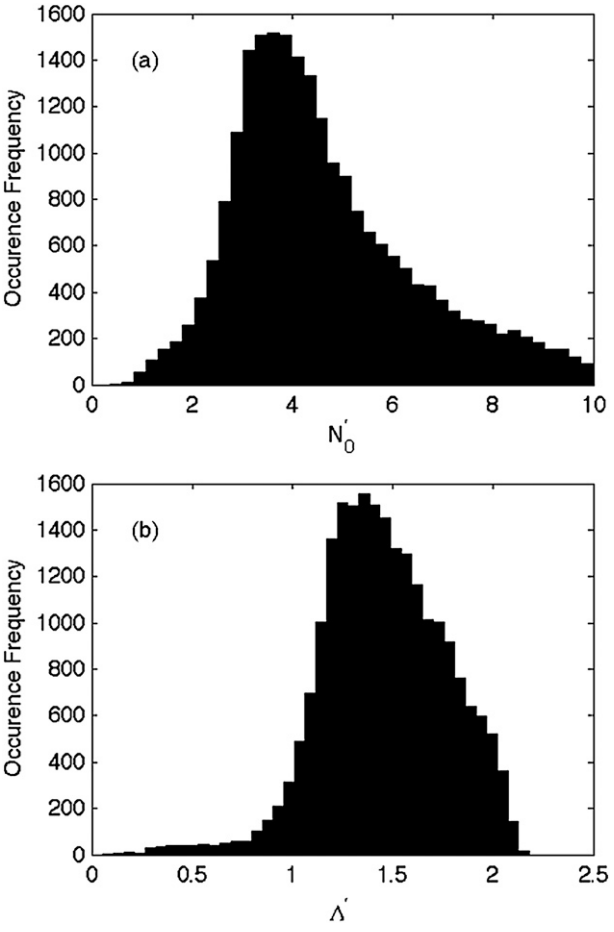

FIG. 3. Histogram of estimated DSD parameters based on 2DVD data: (a) N_0' [$\log_{10}(\text{mm}^{-1-\mu}\,\text{m}^{-3})$] and (b) Λ' ($\text{mm}^{-1/4}$).

of N_0 and Λ. Also, moderate/heavy rain (e.g., $0 < \Lambda < 3\ \text{mm}^{-1}$) now accounts for a larger proportion of the dynamic range than before. It is worth noting that skewed distributions of N_0 and Λ become approximate Gaussian distributions when expressed as N_0' and Λ', implying that N_0' and Λ' are less affected by the biases in N_0 and Λ estimates (typically overestimates).

To obtain the joint distribution of state parameters, we first discretized N_0' with an interval of 0.1 $\log_{10}(\text{mm}^{-1-\mu}\,\text{m}^{-3})$ and Λ' with an interval of 0.05 $\text{mm}^{-1/4}$ to construct grids of N_0' and Λ'. On the basis of estimated parameters of $N_0'$and Λ', the occurrence frequency was counted for each grid. Figure 4 shows the result. The most frequently retrieved N_0'–Λ' pairs have an N_0' value between 3 and 5 $\log_{10}$ ($\text{mm}^{-1-\mu}\,\text{m}^{-3}$) (i.e., N_0 is approximately 10^3–$10^5\ \text{m}^{-3}\ \text{mm}^{-1}$) and a Λ' value between 1.1 and 1.6 $\text{mm}^{-1/4}$ (i.e., Λ is approximately 1.5–6 mm^{-1}). The joint *a prior* PDF of N_0' and Λ' is equal to the normalization of this distribution. It comes entirely from the disdrometer observation and is free of any mathematical function, representing the actual prior distribution.

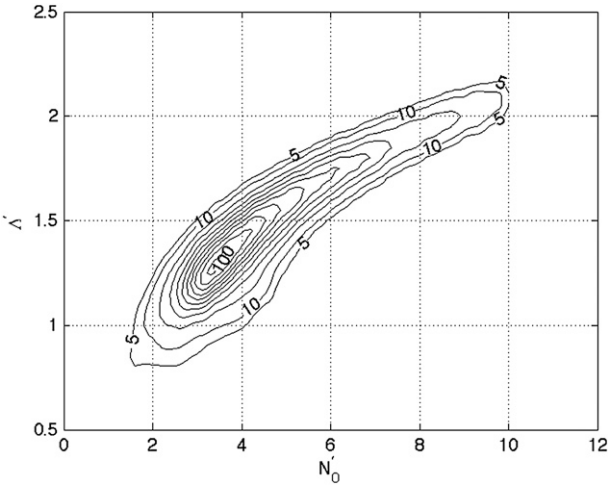

FIG. 4. Contour plot of the occurrence frequency of joint estimated DSD parameters N_0' [$\log_{10}(\mathrm{mm}^{-1-\mu}\,\mathrm{m}^{-3})$] and Λ' ($\mathrm{mm}^{-1/4}$). Interval of unmarked contours between 10 and 100 is 10.

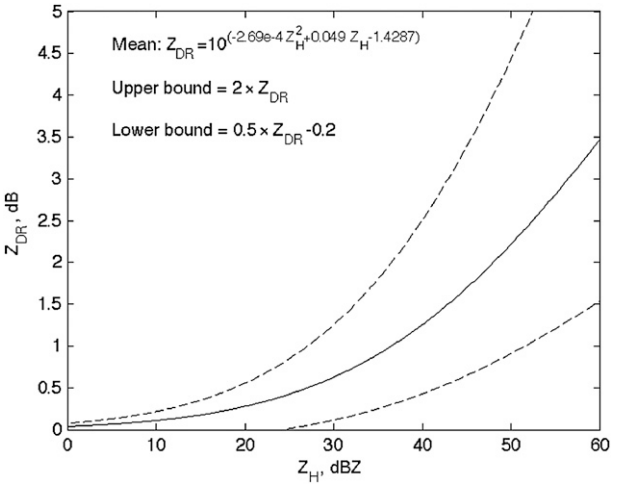

FIG. 5. Sketch of Z_{DR} (dB) vs Z_H (dBZ) from 2DVD measurements. Solid line denotes the mean curve [Eq. (15) of Cao et al. 2008]. Upper and lower bounds (dashed lines) are given according to the mean curve.

d. The conditional distribution

Analogous to the forward model used in the optimal estimation theory, $P_f(\mathbf{y}|\mathbf{x})$ is a bridge between the measurement and state parameter. Generally, it is difficult to find an exact PDF to characterize the measurement with a given DSD. The conditional PDF in the current study is assumed to follow a bivariate normal distribution as

$$P_f(Z_H, Z_{\mathrm{DR}}|\Lambda', N_0') = \frac{1}{2\pi\sigma_{Z_H}\sigma_{Z_{\mathrm{DR}}}(1-\rho^2)^{1/2}} \exp\left\{-\frac{1}{2(1-\rho^2)}\left[\frac{(Z_H-\eta_{Z_H})^2}{\sigma_{Z_H}^2} - \frac{2\rho(Z_H-\eta_{Z_H})(Z_{\mathrm{DR}}-\eta_{Z_{\mathrm{DR}}})}{\sigma_{Z_H}\sigma_{Z_{\mathrm{DR}}}} + \frac{(Z_{\mathrm{DR}}-\eta_{Z_{\mathrm{DR}}})^2}{\sigma_{Z_{\mathrm{DR}}}^2}\right]\right\}, \quad (10)$$

where η is the expected value, and σ^2 indicates the variance. This equation gives a probability model of observed Z_H and Z_{DR} given N_0' and Λ'. The variable ρ in Eq. (10) denotes the correlation coefficient between Z_H and Z_{DR} errors. The error should include both observation and model errors. Generally, observations of Z_H and Z_{DR} could be considered to have independent observation errors. Most previous Bayesian studies have only considered the observation error and assumed $\rho = 0$; however, the model error has seldom been taken into account in those studies. In this study, the C-G DSD model is applied to estimate Z_H and Z_{DR} in the forward operator. It is understood that the forward model might introduce the model error, which tends to be correlated for these two variables. Instinctively, ρ should not equal zero and should vary with different Z_H–Z_{DR} pairs. It is normally not easy to estimate this kind of correlation for each Z_H–Z_{DR} pair. Fortunately, it is found that the effect of ρ on the retrieval is not essential. For the sake of simplicity, this study assumes a constant $\rho = 0.5$, which denotes a moderate correlation between the errors of two variables, for the application of Eq. (10).

Theoretically, σ^2 in Eq. (10) stands for the error variance of the forward models and measurement errors. This study assumes a simple model for this parameter. First, the conditional PDF of Eq. (10) is assumed to work in the logarithm domain; that is, Z_H and Z_{DR} are in units of dBZ and dB, respectively. Considering that Z_H is generally more reliable than other PRD, and its measurement error is generally accepted as 1–2 dB, here, σ_{Z_H} is assumed to be constant at 2 dB, and $\sigma_{Z_{\mathrm{DR}}}$ is assumed to be a function of Z_H and Z_{DR}. Figure 10 of Cao et al. (2008) shows that disdrometer Z_H and Z_{DR} for rain data mostly fall in a bounded region. Dashed lines shown in Fig. 5 give the upper boundary and lower boundary of such a region. Within the bounded region, we assume $\sigma_{Z_{\mathrm{DR}}}$ to be constant at 0.3 dB. If observed PRD fall outside of this region, $\sigma_{Z_{\mathrm{DR}}}$ is believed to be larger than the

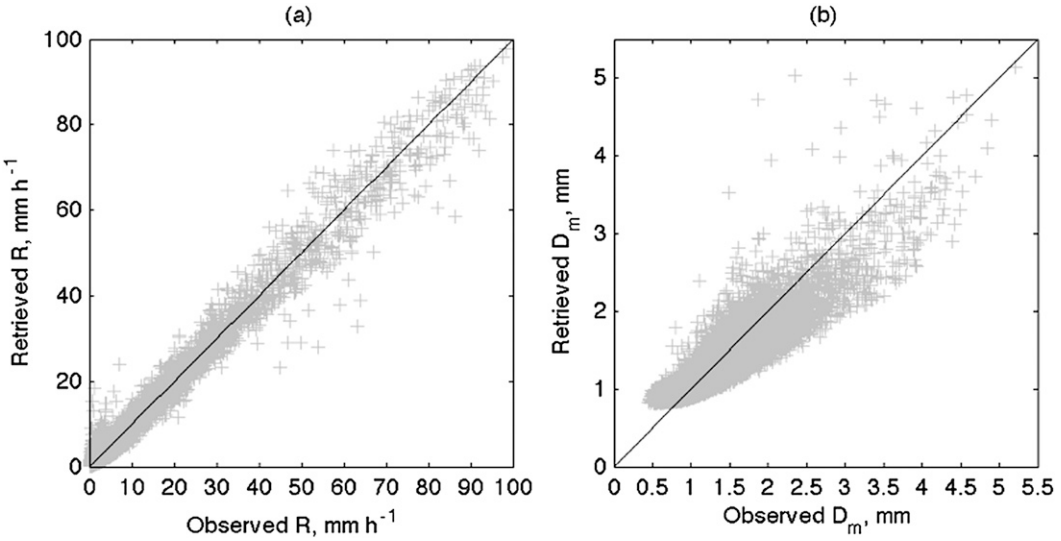

FIG. 6. Scatterplots of retrieved values vs observations: (a) R (mm h^{-1}) and (b) D_m (mm). Crosses represent data points, and solid lines represent equal values of axes.

one inside the region. This assumption is reasonable, because normal $Z_{\rm DR}$ should have a small observation error, while abnormal $Z_{\rm DR}$ could be attributed to a large observation error. The $\sigma_{Z_{\rm DR}}$ value is given by a function as

$$\sigma_{Z_{\rm DR}} = \begin{cases} 0.3(Z_{\rm DR} - Z_{\rm DR}^{\rm up}) + 0.3 & \text{above upper boundary} \\ 0.3 & \text{within the region} \\ 0.3(Z_{\rm DR}^{\rm low} - Z_{\rm DR}) + 0.3 & \text{below lower boundary} \end{cases}, \tag{11}$$

where $Z_{\rm DR}^{\rm up}$ ($Z_{\rm DR}^{\rm low}$) denotes the upper (lower) boundary. Equation (11) implies that if an observed $Z_{\rm DR}$ deviates from the normal range of rain data, $Z_{\rm DR}$ would be less reliable to represent rain.

In brief, the procedure for the Bayesian retrieval is described as follows. Given Z_H and $Z_{\rm DR}$, the conditional probability can be calculated by Eqs. (10) and (11) for either N_0' and Λ'. Knowing the *a prior* PDF of state parameters, mean values and standard deviations of N_0' and Λ' are retrieved by applying Eqs. (4) and (5). Next, the gamma DSD is constructed using retrieved mean values $E(N_0')$ and $E(\Lambda')$ with μ obtained from Eq. (2). Finally, rain variables of interest can be calculated from the retrieved gamma DSD.

4. Evaluation by disdrometer

The Bayesian approach has been evaluated using radar measurements calculated from 2DVD data. Generally, observed DSDs contain measurement errors. Since we do not know the truth of real DSDs, we have assumed observed DSDs to be an approximation of the truth. To make this assumption work, we have rejected DSDs in which the number of drops is less than 50, which are thought to have a large observation error, leaving approximately 24 500 1-min DSDs for the evaluation. Using these DSDs, Z_H and $Z_{\rm DR}$ were simulated based on Eqs. (6) and (7). The simulated Z_H and $Z_{\rm DR}$ were then used to retrieve DSD parameters. Figure 6 shows the plots of retrieved R and D_m versus those obtained from observations. The cross points represent results for every 1-min DSD. As Fig. 6 shows, other than some moderate scattering, retrieved R and D_m match the observations quite well. The correlation coefficients between observation and retrieval values of R and D_m are 0.98 and 0.89, respectively. The scattering increases with increasing R (or D_m), and especially for increasing D_m. The scattering of data points can likely be attributed to the fact that some DSDs are not approximated well by a gamma distribution. For example, there is an obviously large scattering of data points for observed $D_m < 3$ mm and retrieved $D_m > 3.5$ mm. These data points generally have a concave DSD and fewer median size raindrops (or a long tail—that is, a flat high end), which are not sufficient to form a gamma distribution. A simulation from Smith et al. (2009) illustrates one of these cases—that is, the DSD with a long tail (see Fig. 7 in Smith et al. 2009). On the other hand, the use of a constrained C-G model (i.e., μ–Λ relation) may enlarge the uncertainty of retrieval. In Fig. 6a, there are some data points for which R is greatly overestimated—for example, observed $R < 8$ mm h^{-1} and retrieved $R > 10$ mm h^{-1}. These data points generally represent convex and narrow DSDs with a low concentration of small raindrops ($D < 0.8$ mm). Retrieved

TABLE 1. Bias (%) and rmse (%) of Bayesian retrievals vs 2DVD measurements. Units are millimeters per hour for R and millimeters for D_m.

Retrieval type		R range			
		$0.1 < R < 3$	$3 < R < 15$	$15 < R < 30$	$30 < R < 100$
R	Bias	11.9	1.76	−0.64	−1.19
	Rmse	49.7	17.3	11.5	21.5
D_m	Bias	−5.02	−4.43	0.74	8.93
	Rmse	17.3	15.2	13.6	18.7

DSDs under the constraint of μ–Λ relation generally have more small raindrops than the observation, leading to a larger R value.

Although the DSD model error might degrade the retrieval, the overall performance of the Bayesian retrieval algorithm was satisfactory. Table 1 lists the bias and rmse of retrieval versus observation for four ranges of rainfall rate (i.e., $0.1 < R < 3$ mm h^{-1}; $3 < R < 15$ mm h^{-1}; $15 < R < 30$ mm h^{-1}; $30 < R < 100$ mm h^{-1}). Table 1 shows that R tends to be overestimated, and the overestimation is greatest for $R < 3$ mm h^{-1}. On the other hand, D_m tends to be underestimated for $R < 15$ mm h^{-1} and overestimated for $R > 30$ mm h^{-1}. The estimation of R has more uncertainty for light rain (i.e., $R < 3$ mm h^{-1}). A possible reason for this is that DSDs of light rain have a smaller number of raindrops, which may lead to a larger measurement or model error. Apart from light rain, the bias of the R estimate is less than 2%, and the rmse is lower than 22%; that is, the uncertainty of rain estimation is generally no more than 1 dB, which is less than the approximately 2 dB uncertainty of radar measurements.

Figure 7 shows the occurrence histograms of estimated SD(·) values of state variables for four R ranges. The histogram is calculated from SD(·) values retrieved with Eq. (5). Here, **y** has been calculated from the DSD dataset with a specific R range (e.g., $3 < R < 15$ mm h^{-1}). As Fig. 7 shows, estimated SD(·) values tend to decrease with increasing R, implying that estimated state variables have less uncertainty. Because the measurement error has been modeled with σ_{Z_H} and $\sigma_{Z_{DR}}$ in Eq. (10), the retrieved SD(Λ') and SD(N_0') represent the error effect of Z_H and Z_{DR}. Higher SD(·) values denote a larger error effect in the retrieval. Therefore, the SD(·) value could be regarded as an indicator of data quality. Given the real radar data, if estimated SD(·) values are beyond the range for corresponding rainfall rate, it is likely that the data are not for pure rain and might be contaminated. Because Λ is familiar to the community, Fig. 8 shows the analysis of SD(Λ)—that is, the dependence of $E(\Lambda)$ and SD(Λ) on the ratio of Z_{DR}:Z_H. It is worth noting that SD(Λ') and SD(N_0') also have a similar trend to SD(Λ) (not shown). As Figs. 8a and 8b show, the normalized SD(Λ) [i.e., SD(Λ)/$E(\Lambda)$] increases with increasing Z_{DR}:Z_H after it reaches a minimum for some Z_{DR}:Z_H. For a large Z_{DR}:Z_H (e.g., >0.07), the normalized SD(Λ) increases much faster than the one for a small ratio value. Figures 8a and 8b imply that Z_{DR} and Z_H of rain signal have an intrinsic relationship. The uncertainty of retrieved DSD parameters, such as Λ, would be greater if Z_{DR} and Z_H were apart from that relationship. In other words, if retrieved SD(·) values are small, it is likely that the radar data represent the rain signal. Similar to Figs. 8a and 8b, Figs. 8c and 8d show mean curves for different R ranges. All the categories have a very similar tendency for the curve of $E(\Lambda)$ and normalized SD(Λ). Generally speaking, the larger Z_{DR}:Z_H is, the smaller $E(\Lambda)$ is. SD(Λ) has the similar tendency only for the ratio larger than a certain value. One advantage of Bayesian retrieval is the provision of SD(·) values. Figures 7 and 8 demonstrate the characteristics of SD(Λ), which provide the additional information for the confidence/reliability of rain retrieval.

5. Verification by real data

In this section we examine the retrieval algorithm by applying it to real PRD. To verify the Bayesian algorithm, retrieved rainfall rates and 1-h rain accumulations have been compared with gauge measurements, which are supposed to be the ground truth. Two empirical rain estimators have also been compared with the Bayesian algorithm. One empirical estimator, used by WSR-88D as a default estimator for midlatitude rain, is based only on Z_H. The other one is an estimator based on Z_H and Z_{DR}. The two relations are

$$R(Z_H) = 0.017 Z_H^{0.714} \quad \text{and} \tag{12}$$

$$R(Z_H, Z_{DR}) = 0.0142 Z_H^{0.77} Z_{DR}^{-1.67}, \tag{13}$$

respectively. Equation (13) was developed by NSSL for polarimetric radar applications. It had an optimum performance for rain during the Joint Polarization Experiment (JPOLE) field campaign (Ryzhkov et al. 2005b). Before the comparison, a short description of radar data quality control is given as follows.

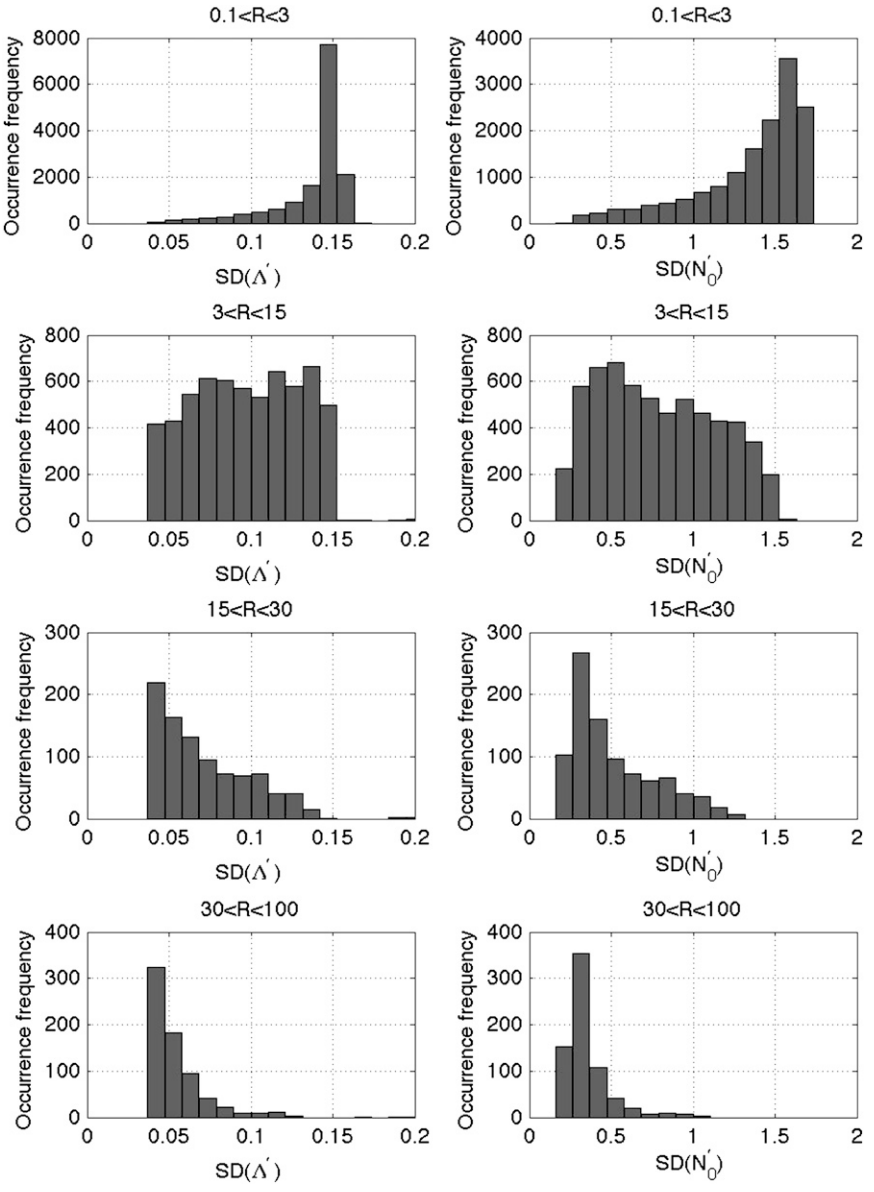

FIG. 7. Occurrence histogram of retrieved SD of (left) Λ' ($\text{mm}^{-1/4}$) and (right) N_0' [$\log_{10}(\text{mm}^{-1-\mu}\,\text{m}^{-3})$]. (top)–(bottom) Data within the range of $0.1 < R < 3$, $3 < R < 15$, $15 < R < 30$, and $30 < R < 100$ mm h^{-1}, respectively.

a. Radar data quality control

To smooth the data and reduce speckling, a filtering procedure (see the appendix) was performed on the radar-measured Z_H and Z_V. Filtered Z_{DR} was calculated from filtered Z_H and Z_V. Because verification was conducted only for pure rain, we eliminated radar pixels contaminated by hail, anomalous propagation, and biological scatters. This task was accomplished with a hydrometeor classification algorithm developed by NSSL (Schuur et al. 2003). The eliminated data point was replaced by the average of uncontaminated Z_H and Z_{DR} measurements within a 1-km distance. If the contaminated area was large (e.g., beyond a 1-km distance), then Z_H and Z_{DR} were estimated by interpolating Z_H and Z_{DR} measurements from adjacent uncontaminated regions.

As discussed in the introduction, radar measurements were calibrated using 2DVD data. For the rain event on 13 May 2005, Fig. 9 shows time series evolutions of uncalibrated Z_H and Z_{DR} (classified as pure rain) from radar, as well as Z_H and Z_{DR} computed from the 2DVD observation. After interpolating radar data into a 1-min

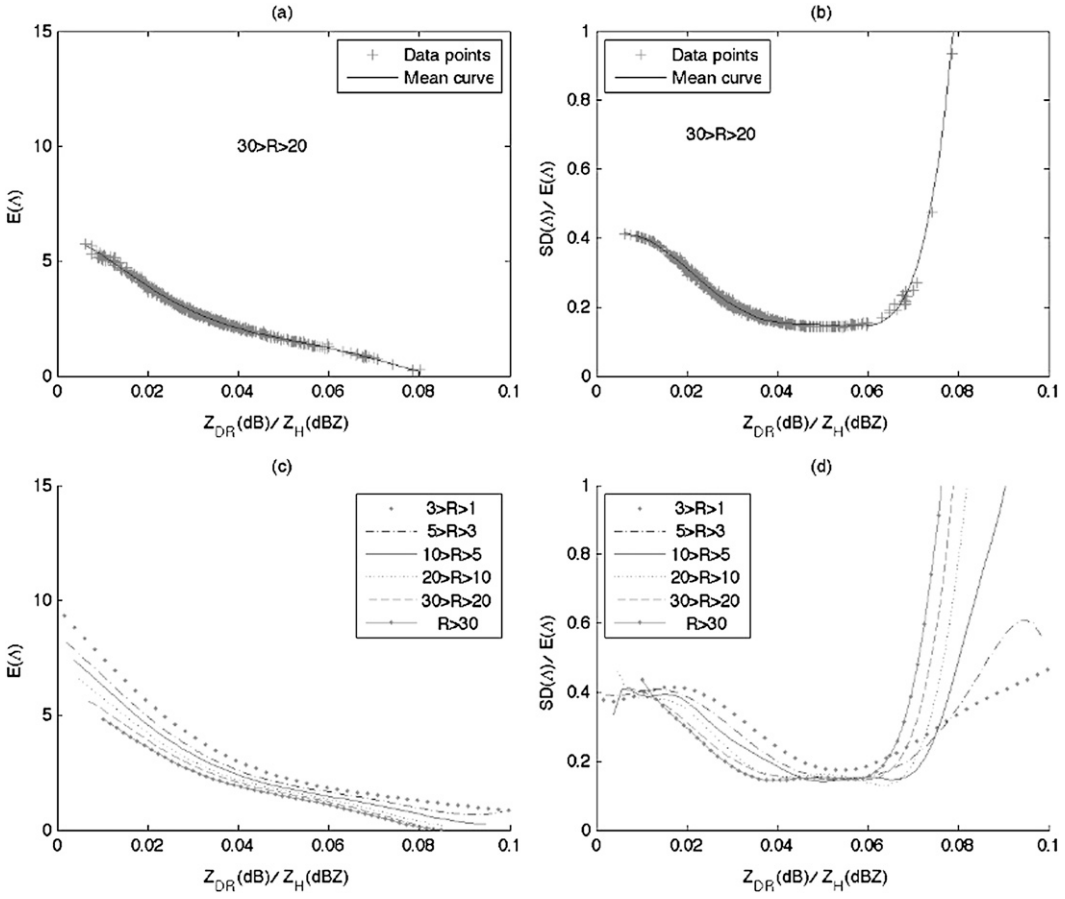

FIG. 8. Dependence of $E(\Lambda)$ (mm^{-1}) and SD(Λ) (mm^{-1}) on the ratio $Z_{\rm DR}$ (dB):Z_H (dBZ) (a),(b) Mean curve fitted to the data points of $20 < R < 30$ mm h^{-1}. (c),(d) Display mean curves associated with data points of $1 < R < 3$, $3 < R < 5$, $5 < R < 10$, $10 < R < 20$, $20 < R < 30$, and $30 < R$ (mm h^{-1}), respectively.

time scale, the difference between the two lines was calculated and averaged for the period from 0700 to 1300 UTC. The averaged difference was found to be −1.08 dB (radar lower) for Z_H and 0.36 dB for $Z_{\rm DR}$. Radar-measured Z_H and $Z_{\rm DR}$ were then calibrated by subtracting these biases before the Bayesian retrieval was applied.

Figure 10 shows a retrieval based on KOUN radar observations presented in Fig. 2. Figure 10a shows a PPI of R from the Bayesian retrieval, which has been filtered with the classification presented in Fig. 2d, The R field from the empirical dual-polarized (dual-pol) retrieval using Eq. (13) (not shown) is similar to Fig. 10a. Figure 10b shows R from the empirical single-polarized (single-pol) retrieval using Eq. (12). Figure 10b contains some speckles to the southeast of the storm's leading edge that were not filtered out by the speckle filter. Those speckles are likely due to normally biological echoes that were rejected by the classification filter applied to Fig. 10a. Although Figs. 10a and 10b exhibit similar storm features and rainfall rates within the stratiform region, Fig. 10b has a higher rainfall rate than Fig. 10a for the region of strong convection. Figures 10c and 10d display images of SD(Λ') and SD(N_0') from the Bayesian retrieval. Both SD(·) images have a similar trend, implying that either one can be used alone as an indicator of data quality. It is worth noting that both Figs. 10c and 10d have directly applied the radar data shown in Figs. 2a and 2b without the radar echo classification. The SD(·) images are consistent with the classification in Fig. 2d. The rain region typically has small SD(·) values. Values that exceed the normal rain signal ranges are indications of contamination or nonrain in the region. The larger SD(·) value is, the greater uncertainty in the rain retrieval is.

b. Mesonet data verification

Here, we present a comparison of 2DVD and mesonet rain gauge measurements in an attempt to validate the 2DVD measurement used in this study. The WASH rain gauge used in this comparison was located approximately

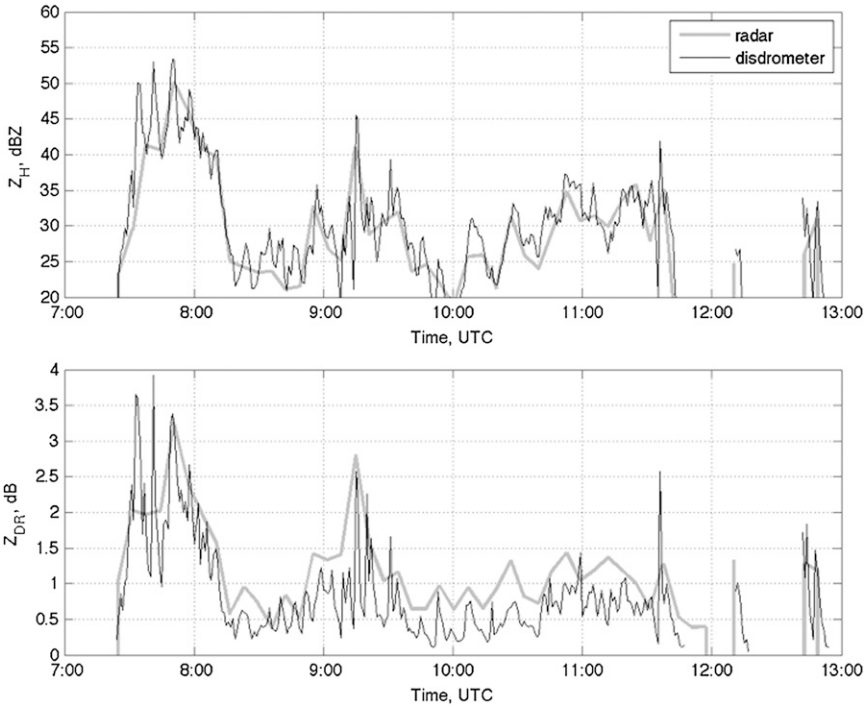

FIG. 9. Time series of (top) Z_H (dBZ) and (bottom) Z_{DR} (dB). Gray line denotes uncalibrated values from radar, and black line denotes values calculated from 2DVDs.

300 m from the 2DVD. Although the rain inhomogeneity and measurement error for both instruments could degrade the comparison, we expect that rainfall rates (accumulations) measured by two instruments should compare well. Figure 11 shows the comparison of 2DVD with mesonet rain gauge for rainfall rate and 1-h rain accumulation on 13 May 2005. The 1-h rain accumulation was calculated by accounting for all rainfall that fell within a 30-min period before and after a given time. Because the 2DVD recorded data every 1 min and the rain gauge recorded rain data every 5 min, 2DVD data were examined at 5-min intervals for consistency. As shown in Fig. 11, temporal variations match well for both rainfall rate and 1-h rain accumulation. The fractional difference of rainfall rate between two instruments is only 3.18%, which is less than the approximately 5% measurement error of rain gauge, which implies that rain gauge and 2DVD measurements are reliable enough to be regarded as the ground truth.

Figure 12 presents a comparison of radar-retrieved rainfall rates with in situ measurements, including rain gauge measurements at six mesonet sites and 2DVD measurements at KFFL. Figure 13 shows a comparison of 1-h rain accumulation at the same location. As can be seen in Figs. 12 and 13, the performance of the Bayesian estimator is similar to that of the dual-pol estimator. Both the Bayesian retrieval and empirical dual-pol retrieval give a satisfactory result that captures the temporal variation of in situ measurement. The single-pol estimator normally overestimates rainfall during the convection while performing fairly well in the stratiform region. It is worth noting that mixtures of rain and hail might exist near the convective core (e.g., near 0655 UTC at MINC), where radar-measured Z_H and Z_{DR} are sometimes extremely large (e.g., $Z_H > 55$ dBZ and $Z_{DR} > 3.5$ dB). If quality control was not performed, the rainfall rate estimated from contaminated Z_H and Z_{DR} would be much larger than 100 mm h^{-1}. In situ measurements in Figs. 12 and 13, however, show that this is not the case. Radar retrievals in Figs. 12 and 13 demonstrate that radar data quality control [i.e., using radar measurements (classified as rain) from an adjacent area to interpolate over a hail-contaminated region] can provide a reasonable rain estimate for the contaminated region.

By comparison, the Bayesian retrieval is superior to the empirical dual-pol retrieval. Both retrievals are better than the single-pol retrieval. As Fig. 13 shows, the empirical dual-pol retrieval tends to overestimate the 1-h rain accumulation for heavy (sometimes moderate) rain. The empirical single-pol (single parameter) retrieval has an even worse performance, especially in the

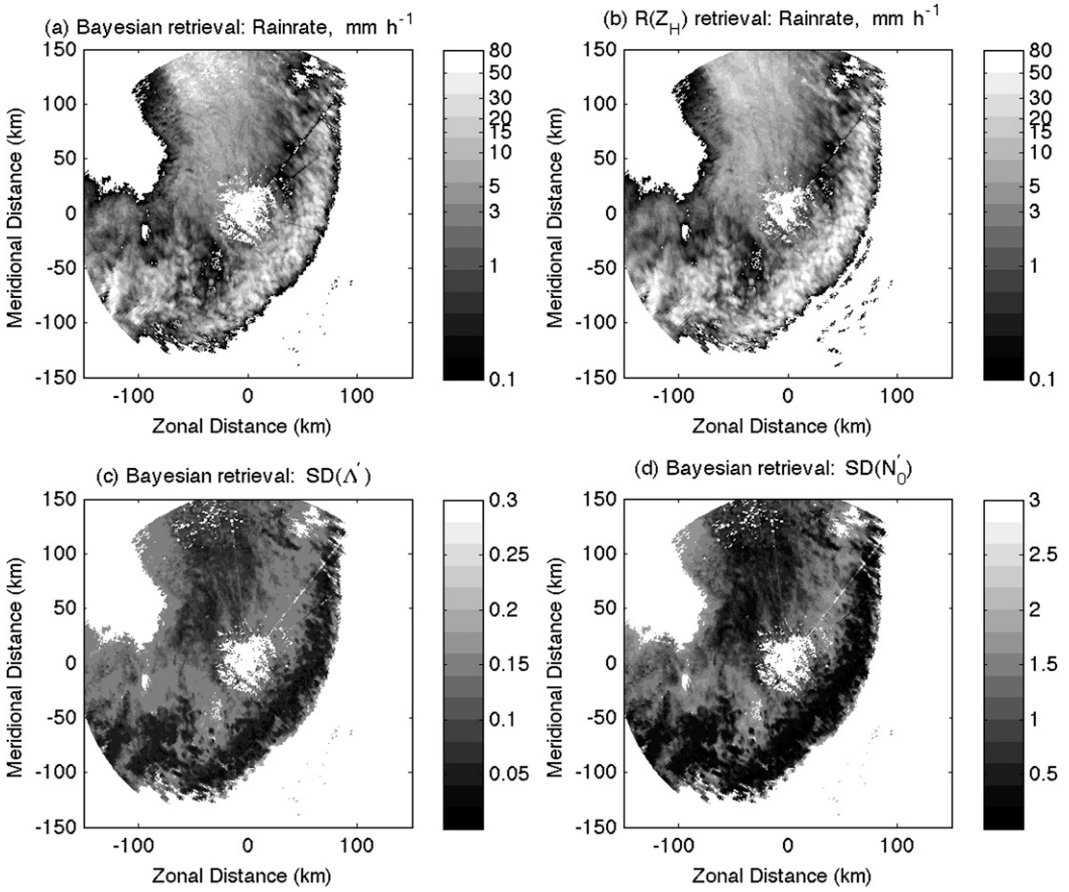

FIG. 10. Retrieval results from radar observations presented in Fig. 2 (i.e., 0830 UTC 13 May 2005): (a) R (mm h^{-1}) from Bayesian retrieval, (b) R (mm h^{-1}) from $R(Z_H)$ retrieval, (c) SD(Λ') ($mm^{-1/4}$) from Bayesian retrieval, and (d) SD(N_0') [$\log_{10}(mm^{-1-\mu}\ m^{-3})$] from Bayesian retrieval.

region of strong convection. Table 2 gives the bias and rmse of the 1-h rain accumulation retrieval. The empirical single-pol retrieval has the worst result. At the seven sites (six mesonet and one disdrometer), the Bayesian retrieval generally has both smaller biases (up to approximately 16%) and rmse (up to approximately 22%) when compared to the empirical retrieval. With the exception of CHIC, the empirical dual-pol retrieval has a larger bias and rmse than the Bayesian retrieval.

6. Discussion and conclusions

The Bayesian approach presented in this study is limited to two polarimetric variables: Z_H and Z_{DR}. It is possible to incorporate other polarimetric measurements—such as correlation coefficient and differential phase—to improve the effectiveness of the algorithm; however, an appropriate conditional distribution model representing additional variables [i.e., Eq. (10)] is required, causing the complexity of this approach to increase. It is worth noting that the approach introduced here incorporates historic information and does not apply spatial information (as in some other studies). The attenuation correction algorithm that applies spatial information is beyond the scope of this study. A variational method could be a good candidate to solve this kind of problem (e.g., Hogan 2007; Cao et al. 2009; Xue et al. 2009).

Results of this study show that the proposed Bayesian approach is effective as long as radar measurements match disdrometer measurements. If we trust disdrometer measurements and related raindrop-scattering theory, then radar measurements should exhibit such a consistency with disdrometer measurements, ignoring error effects due to the scattering-model error and the sampling error. The calibration to raw radar data mitigates the error effect that degrades the quantitative interpretation of radar observation using the scattering theory. The case study presented in section 5 also shows the consistency between the rain gauge and disdrometer. This suggests that rain gauge data, which are widely available

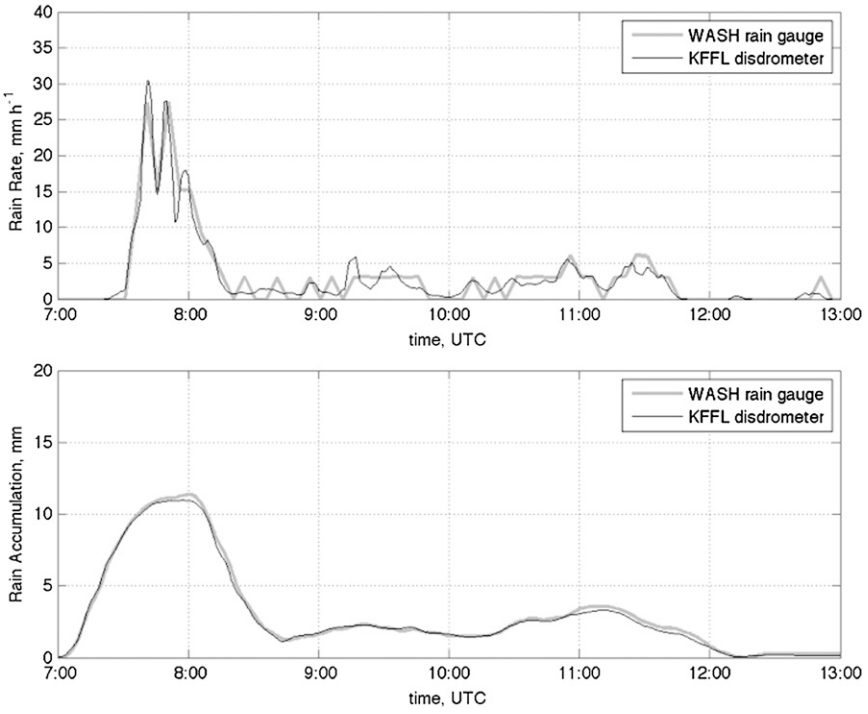

FIG. 11. Rain comparison between measurements from disdrometer and mesonet rain gauge: (a) R (mm h^{-1}) and (b) 1-h rain accumulation (mm). The 1-h rain accumulation at a given time was calculated by accounting for the rainfall within 30 min before and after this time.

nationwide, can be considered as another source for radar calibration in practical applications.

In this study, rain estimation has been performed for the first time by applying a Bayesian approach in which C-G DSD parameters are estimated from Z_H and Z_{DR}. The *a prior* PDF of state parameter is constructed using 2DVD measurements collected in central Oklahoma over a 3-yr period. The conditional PDF is assumed to follow a bivariate Gaussian model. This assumption comes from the general property of DSD moments, which have an approximately Gaussian distribution in the logarithmic domain (Zhang et al. 2008). The estimation of radar measurements (i.e., forward model) is based on raindrop backscattering theory. The DSD model—as well as other assumptions, such as raindrop shape, temperature, and oscillation—is applied in the forward model. Although these assumptions may have an error, the retrieval result suggests that they work well for rain estimation. Here, 2DVD and rain gauge measurements have been regarded as the ground truth. An example presented in Fig. 11 shows that a 2DVD and a rain gauge, which have been located at a distance of approximately 300 m, provide very similar measurements of rainfall rate and rain accumulation, thereby demonstrating the reliability of both instruments. As a result of this consistency, the Bayesian retrieval could be verified by ground measurements at seven places (i.e., one 2DVD site and six mesonet rain gauge sites). A comparison of retrieval results with observations has demonstrated that retrieved rainfall rates and 1-h rain accumulations match in situ measurements, as well as temporal variations, well. In addition, it is shown that the Bayesian approach is essentially consistent with the empirical dual-pol relation [i.e., Eq. (13)]. The consistency comes from the fact that both approaches are mainly based on Z_H and Z_{DR}; however, the Bayesian retrieval, which does not use deterministic coefficients, performs better. It gives an estimate with the maximum posterior probability, as well as the standard deviation of estimation, which can be used as a good indicator of radar data quality. We therefore believe that the Bayesian approach has the potential to improve the rain estimation from polarimetric radar measurements.

Acknowledgments. This work was supported by the National Science Foundation (NSF) Grant ATM-0608168. The participation of E. A. Brandes was supported by funds from the NSF designated for the U.S. Weather Research Program at NCAR. The authors greatly appreciate Kyoko Ikeda at NCAR, who collected NCAR 2DVD data, and Dr. C. A. Fiebrich at Oklahoma Climatological Survey, who provided the mesonet rain gauge

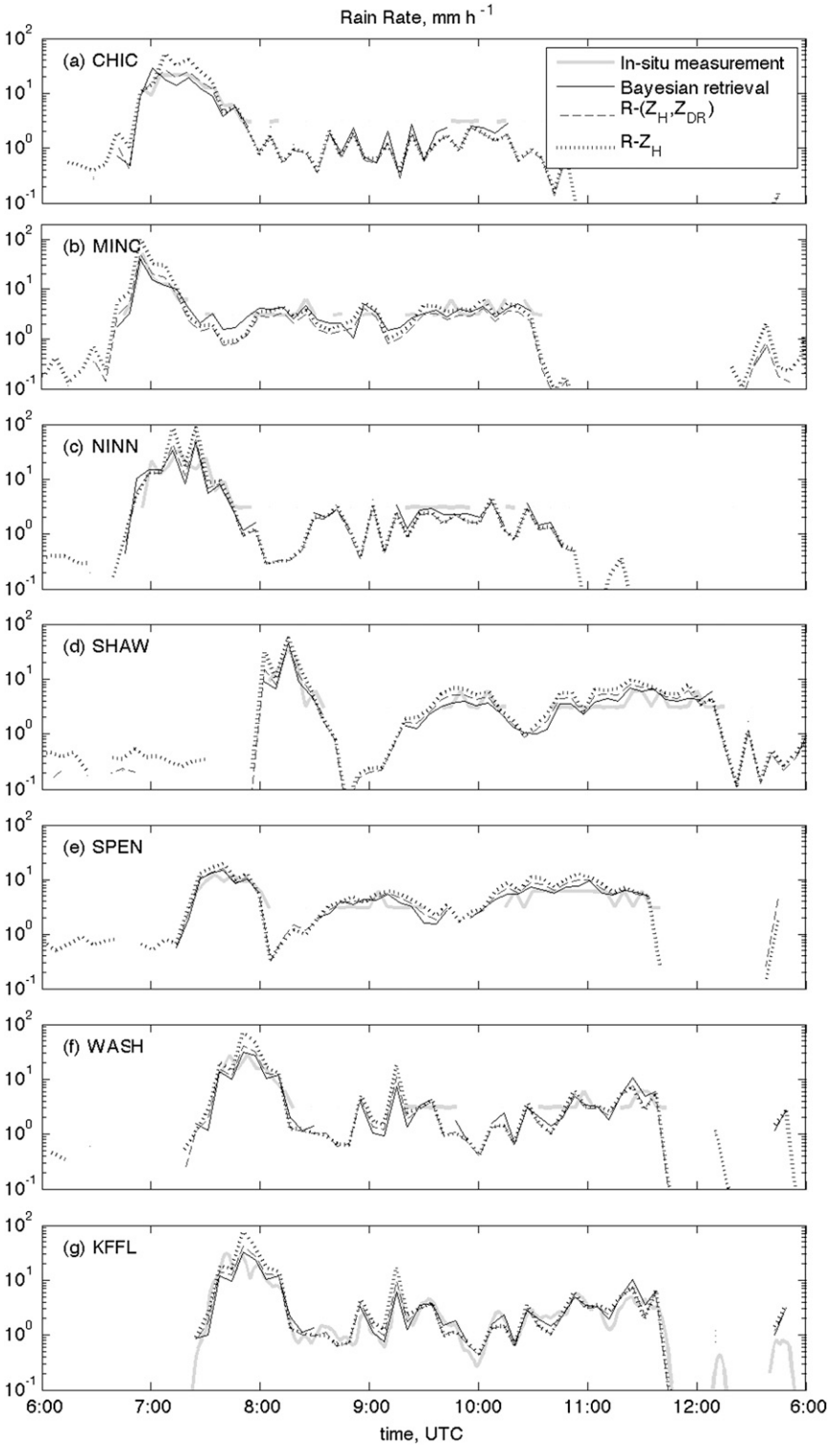

FIG. 12. Comparisons of R (mm h^{-1}) between radar retrievals and in situ measurements at seven sites: (a) CHIC, (b) MINC, (c) NINN, (d) SHAW, (e) SPEN, (f) WASH, and (g) KFFL.

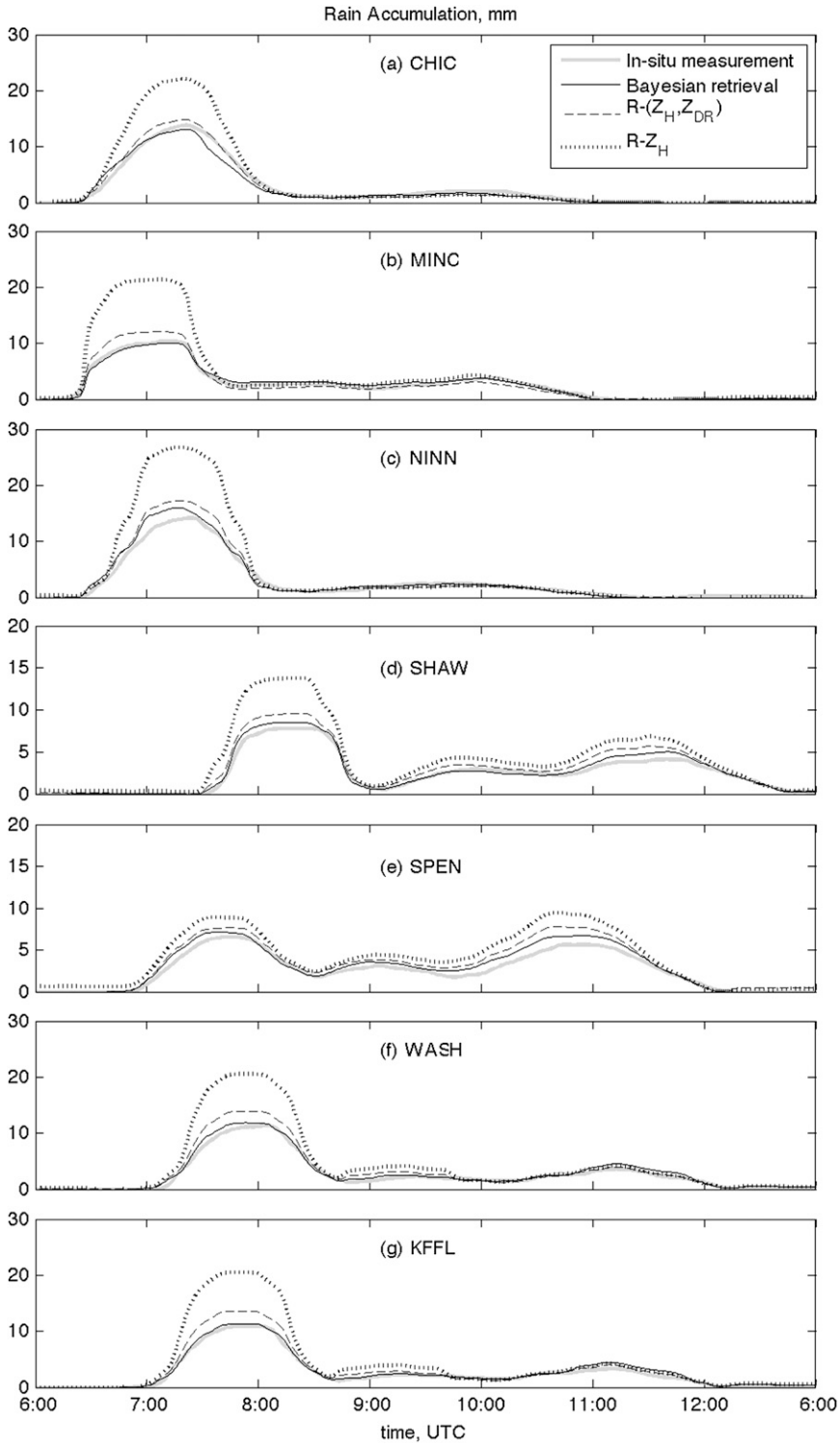

FIG. 13. As in Fig. 12 but for 1-h rain accumulation (mm) of radar retrievals and in situ measurements.

TABLE 2. Bias (%) and rmse (%) of rain retrievals (1-h rain accumulation) vs in situ measurements at sites.

Retrieval type		CHIC	MINC	NINN	SHAW	SPEN	WASH	KFFL
Bayesian	Bias	−7.3	2.5	8.3	7.8	15.5	10.7	10.0
	Rmse	21.0	11.5	21.7	14.7	19.6	16.4	15.5
Empirical $R(Z_H, Z_{DR})$	Bias	1.1	1.6	12.3	22.4	28.0	19.8	20.2
	Rmse	17.3	26.4	33.5	29.9	33.9	34.4	33.3
Empirical $R(Z_H)$	Bias	35.4	48.1	48.2	49.5	44.9	48.9	50.4
	Rmse	80.4	103.5	106.8	72.3	56.0	95.3	92.5

data. The authors also are thankful for the help of radar engineers at NSSL, who collected the KOUN radar data.

APPENDIX

Filtering Procedure for Z_H and Z_V

The concept of speckle filter applied in this study is similar to the one described by Lee et al. (1997), except for minor changes. Assuming radar reflectivity is combined with a multiplicative noise N, the observation is then expressed in logarithmic domain by

$$Z^O_{H,V}(\mathrm{dB}Z) = Z^T_{H,V}(\mathrm{dB}Z) + N(\mathrm{dB}), \qquad \text{(A1)}$$

where subscripts H and V represent horizontal and vertical polarization, respectively; superscripts O and T denote the observation and the truth, respectively; and N(dB) is assumed to be a random white noise with Gaussian PDF. Therefore, radar reflectivity at horizontal or vertical polarization could be estimated by

$$\hat{Z}^T_{H,V}(\mathrm{dB}Z) = \overline{Z^O_{H,V}}(\mathrm{dB}Z) + b[Z^O_{H,V}(\mathrm{dB}Z) - \overline{Z^O_{H,V}}(\mathrm{dB}Z)], \qquad \text{(A2)}$$

where

$$b = \frac{\mathrm{Var}[Z^T_{H,V}(\mathrm{dB}Z)]}{\mathrm{Var}[Z^O_{H,V}(\mathrm{dB}Z)]} \quad \text{and}$$

$$\mathrm{Var}[Z^T_{H,V}(\mathrm{dB}Z)] = \mathrm{Var}[Z^O_{H,V}(\mathrm{dB}Z)] - \mathrm{Var}[N(\mathrm{dB})]. \qquad \text{(A3)}$$

The Var[·] denotes the variance, and the overbar denotes the mean. In this study, the mean and variance of the observed $Z_{H,V}$ are estimated from observations of adjacent area of distance 1 km. The measurement error [i.e., standard deviation of N(dB)] is assumed to be 2 dB. The minimum variance of $Z_{H,V}$ is assumed to be 1 dB^2; that is, the minimum value of b is set to 0.2.

REFERENCES

Beard, K. V., and C. Chuang, 1987: A new model for the equilibrium shape of raindrops. *J. Atmos. Sci.,* **44,** 1509–1524.

Brandes, E. A., J. Vivekanandan, and J. W. Wilson, 1999: A comparison of radar reflectivity estimates of rainfall from collocated radars. *J. Atmos. Oceanic Technol.,* **16,** 1264–1272.

——, G. Zhang, and J. Vivekanandan, 2002: Experiments in rainfall estimation with a polarimetric radar in a subtropical environment. *J. Appl. Meteor.,* **41,** 674–685.

——, ——, and ——, 2003: An evaluation of a drop distribution–based polarimetric radar rainfall estimator. *J. Appl. Meteor.,* **42,** 652–660.

——, ——, and ——, 2004a: Comparison of polarimetric radar drop size distribution retrieval algorithms. *J. Atmos. Oceanic Technol.,* **21,** 584–598.

——, ——, and ——, 2004b: Drop size distribution retrieval with polarimetric radar: Model and application. *J. Appl. Meteor.,* **43,** 461–475.

——, ——, and ——, 2005: Corrigendum. *J. Appl. Meteor.,* **44,** 186.

Bringi, V. N., V. Chandrasekar, J. Hubbert, E. Gorgucci, W. L. Randeu, and M. Schoenhuber, 2003: Raindrop size distribution in different climatic regimes from disdrometer and dual-polarized radar analysis. *J. Atmos. Sci.,* **60,** 354–365.

Cao, Q., and G. Zhang, 2009: Errors in estimating raindrop size distribution parameters employing disdrometer and simulated raindrop spectra. *J. Appl. Meteor. Climatol.,* **48,** 406–425.

——, ——, E. Brandes, T. Schuur, A. Ryzhkov, and K. Ikeda, 2008: Analysis of video disdrometer and polarimetric radar data to characterize rain microphysics in Oklahoma. *J. Appl. Meteor. Climatol.,* **47,** 2238–2255.

——, ——, and M. Xue, cited 2009: Variational retrieval of raindrop size distribution from polarimetric radar data in presence of attenuation. [Available online at http://ams.confex.com/ams/89annual/techprogram/paper_144407.htm.]

Chiu, J. C., and G. W. Petty, 2006: Bayesian retrieval of complete posterior PDFs of oceanic rain rate from microwave observations. *J. Appl. Meteor. Climatol.,* **45,** 1073–1095.

Ciach, G. J., 2003: Local random errors in tipping-bucket rain gauge measurements. *J. Atmos. Oceanic Technol.,* **20,** 752–759.

——, and W. F. Krajewski, 2006: Analysis and modeling of spatial correlation structure in small-scale rainfall in central Oklahoma. *Adv. Water Resour.,* **29,** 1450–1463.

Di Michele, S., A. Tassa, A. Mugnai, F. S. Marzano, P. Bauer, and J. P. V. P. Baptista, 2005: Bayesian algorithm for microwave-based precipitation retrieval: Description and application to TMI measurements over ocean. *IEEE Trans. Geosci. Remote Sens.,* **43,** 778–791.

Evans, K. F., J. Turk, T. Wong, and G. L. Stephens, 1995: A Bayesian approach to microwave precipitation profile retrieval. *J. Appl. Meteor.,* **34,** 260–279.

Gorgucci, E., V. Chandrasekar, V. N. Bringi, and G. Scarchilli, 2002: Estimation of raindrop size distribution parameters from polarimetric radar measurements. *J. Atmos. Sci.,* **59,** 2373–2384.

Habib, E., W. F. Krajewski, and A. Kruger, 2001: Sampling errors of tipping-bucket rain gauge measurements. *J. Hydrol. Eng.,* **6,** 159–166.

Hogan, R. J., 2007: A variational scheme for retrieving rainfall rate and hail reflectivity fraction from polarization radar. *J. Appl. Meteor. Climatol.,* **46,** 1544–1564.

Kruger, A., and W. F. Krajewski, 2002: Two-dimensional video disdrometer: A description. *J. Atmos. Oceanic Technol.,* **19,** 602–617.

Lee, G., 2006: Sources of errors in rainfall measurements by polarimetric radar: Variability of drop size distributions, observational noise, and variation of relationships between *R* and polarimetric parameters. *J. Atmos. Oceanic Technol.,* **23,** 1005–1028.

——, and I. Zawadzki, 2005: Variability of drop size distributions: Time-scale dependence of the variability and its effects on rain estimation. *J. Appl. Meteor.,* **44,** 241–255.

——, and ——, 2006: Radar calibration by gage, disdrometer, and polarimetry: Theoretical limit caused by the variability of drop size distribution and application to fast scanning operational radar data. *J. Hydrol.,* **328,** 83–97.

Lee, J. S., M. R. Grunes, and G. De Grandi, 1997: Polarimetric SAR speckle filtering and its impact on classification. *Proc. IGARSS '97: Remote Sensing—A Scientific Vision for Sustainable Development,* Singapore, IEEE, Vol. 2, 1038–1040.

McFarlane, S. A., K. F. Evans, and A. S. Ackerman, 2002: A Bayesian algorithm for the retrieval of liquid water cloud properties from microwave radiometer and millimeter radar data. *J. Geophys. Res.,* **107,** 4317, doi:10.1029/2001JD001011.

Rosenfeld, D., and C. W. Ulbrich, 2003: Cloud microphysical properties, processes, and rainfall estimation opportunities. *Radar and Atmospheric Science: A Collection of Essays in Honor of David Atlas, Meteor. Monogr.,* No. 30, 237–258.

Ryzhkov, A. V., S. E. Giangrande, V. M. Melnikov, and T. J. Schuur, 2005a: Calibration issues of dual-polarization radar measurements. *J. Atmos. Oceanic Technol.,* **22,** 1138–1155.

——, ——, and T. J. Schuur, 2005b: Rainfall estimation with a polarimetric prototype of WSR-88D. *J. Appl. Meteor.,* **44,** 502–515.

——, T. J. Schuur, D. W. Burgess, P. L. Heinselman, S. E. Giangrande, and D. S. Zrnic, 2005c: The Joint Polarization Experiment: Polarimetric rainfall measurements and hydrometeor classification. *Bull. Amer. Meteor. Soc.,* **86,** 809–824.

Sachidananda, M., and D. Zrnić, 1987: Rain rate estimates from differential polarization measurements. *J. Atmos. Oceanic Technol.,* **4,** 588–598.

Schuur, T. J., A. V. Ryzhkov, D. S. Zrnić, and M. Schönhuber, 2001: Drop size distributions measured by a 2D video disdrometer: Comparison with dual-polarization radar data. *J. Appl. Meteor.,* **40,** 1019–1034.

——, ——, P. L. Heinselman, D. S. Zrnić, D. W. Burgess, and K. A. Scharfenberg, 2003: Observations and classification of echoes with the polarimetric WSR-88D radar. National Severe Storms Laboratory Rep., 46 pp. [Available online at http://publications.nssl.noaa.gov/wsr88d_reports/JPOLE_Obs_and_Classification_of_Echoes_Report.pdf.]

Smith, P. L., D. V. Kliche, and R. W. Johnson, 2009: The bias and error in moment estimators for parameters of drop size distribution functions: Sampling from gamma distributions. *J. Appl. Meteor. Climatol.,* **48,** 2118–2126.

Steiner, M., J. A. Smith, and R. Uijlenhoet, 2004: A microphysical interpretation of radar reflectivity–rain rate relationships. *J. Atmos. Sci.,* **61,** 1114–1131.

Vivekanandan, J., G. Zhang, and E. Brandes, 2004: Polarimetric radar rain estimators based on constrained gamma drop size distribution model. *J. Appl. Meteor.,* **43,** 217–230.

Xue, M., M. Tong, and G. Zhang, 2009: Simultaneous state estimation and attenuation correction for thunderstorms with radar data using an ensemble Kalman filter: Tests with simulated data. *Quart. J. Roy. Meteor. Soc.,* **135,** 1409–1423.

Zhang, G., J. Vivekanandan, and E. Brandes, 2001: A method for estimating rain rate and drop size distribution from polarimetric radar. *IEEE Trans. Geosci. Remote Sens.,* **39,** 830–840.

——, ——, ——, R. Menegini, and T. Kozu, 2003: The shape–slope relation in observed gamma raindrop size distributions: Statistical error or useful information? *J. Atmos. Oceanic Technol.,* **20,** 1106–1119.

——, ——, and ——, 2006: Improving parameterization of rain microphysics with disdrometer and radar observations. *J. Atmos. Sci.,* **63,** 1273–1290.

——, M. Xue, Q. Cao, and D. Dawson, 2008: Diagnosing the intercept parameter for exponential raindrop size distribution based on video disdrometer observations: Model development. *J. Appl. Meteor. Climatol.,* **47,** 2983–2992.